Chemical Science

ROYAL SOCIETY OF CHEMISTRY

EDGE ARTICLE

View Article Online
View Journal | View Issue

Cite this: *Chem. Sci.*, 2022, **13**, 781

All publication charges for this article have been paid for by the Royal Society of Chemistry

Stable room temperature ferroelectricity in hydrogen-bonded supramolecular assemblies of ambipolar π-systems†

Anurag Mukherjee,‡[a] Shubhankar Barman,‡[a] Anupam Ghosh,[b] Saptarshi Chakraborty,[a] Ayan Datta, *[b] Anuja Datta *[a] and Suhrit Ghosh *[a]

This article reports H-bonding driven supramolecular polymerization of naphthalimide (A)–thiophene (D)–naphthalimide (A) (AD_nA, $n = 1$–4) conjugated ambipolar π-systems and its remarkable impact on room temperature ferroelectricity. Electrochemical studies confirm the ambipolar nature of these AD_nA molecules with the HOMO–LUMO gap varying between 2.05 and 2.29 eV. Electron density mapping from ESP calculations reveals intra-molecular charge separation as typically observed in ambipolar systems. In the aggregated state, AD_1A and AD_2A exhibit bathochromically shifted absorption bands while AD_3A and AD_4A show typical H-aggregation with a hypsochromic shift. Polarization *vs.* electric field (*P*–*E*) measurements reveal stable room temperature ferroelectricity for these supramolecular assemblies, most prominent for the AD_2A system, with a Curie temperature (T_c) ≈ 361 K and saturation polarization (P_s) of ~2 μC cm^{-2} at a rather low coercive field of ~2 kV cm^{-1}. Control molecules, lacking either the ambipolar chromophore or the amide functionality, do not show any ferroelectricity, vindicating the present molecular and supramolecular design. Computational studies enable structural optimization of the stacked oligomer(s) of AD_2A molecules and reveal a significant increase in the macro-dipole moment (in the range of 10–12 Debye) going from the monomer to the oligomer(s), which provides the rationale for the origin of ferroelectricity in these supramolecular polymers.

Received 20th August 2021
Accepted 17th December 2021

DOI: 10.1039/d1sc04617a

rsc.li/chemical-science

Introduction

Ferroelectric (FE)-materials possess spontaneously generated reversible electric polarization with diverse applications in electronics, electro-optics and electromechanics.[1] Although the first FE-organic crystal[2] was discovered long ago, to date, purely organic FE-systems are limited to a handful of examples,[3] including crystals,[4] fluorinated polymers,[5] liquid crystals[6] and supramolecular assemblies.[3d] Soft-ferroelectrics are emerging as an essential component for sustainable microelectronics in medical industries or biomechano-interactive information, as they promise to offer distinct advantages for environmentally benign, solution-processed, flexible device fabrication. Organic FE-systems,[3] in most cases, exhibit low to moderate polarization at sub-ambient temperatures and are not yet comparable with the benchmark inorganic perovskites[7,8] or organic–inorganic hybrid compounds.[9] Charge-transfer (CT) complexes[10] of donor (D) and acceptor (A) chromophores were identified for FE-polarization[11] only at sub-ambient temperatures (<71 K), until a recent breakthrough, when H-bonded D–A supramolecular assemblies were recognized for displacive-type FE-polarization at room temperature (rt),[12] owing to the alignment of the CT-dipoles. However, it remains a non-trivial task to regulate the stacking sequence in two-component H-bonded CT-complexes,[13] which plays a decisive role in the FE-response. Such uncertainty may be circumvented if a similar FE-mechanism can be realized in supramolecular polymers[14] of single-component D–A conjugated systems. In fact, such attempts had been made with dipolar molecules,[3a] which did not yield much success because they seldom crystallize to polar solids due to an anti-parallel orientation.[15] Similar issues may not arise in the assembly of ambipolar π-systems,[16] which have been known for charge-transport and in other contexts,[17] but never reported before for ferroelectricity. We envisaged that the intrinsic polarizability of ambipolar chromophores may just be sufficient to provide the required instability in the non-centrosymmetric assembled state for spontaneous deformation under the influence of an external electric field, leading to FE-switching. With this postulate, we have studied a series of

[a]*School of Applied and Interdisciplinary Sciences, Indian Association for the Cultivation of Science, 2A and 2B Raja SC Mallick Road, Jadavpur, Kolkata, 700032, India. E-mail: psusg2@iacs.res.in; psuad4@iacs.res.in*

[b]*School of Chemical Sciences, Indian Association for the Cultivation of Science, 2A and 2B Raja SC Mallick Road, Jadavpur, Kolkata, 700032, India. E-mail: spad@iacs.res.in*

† Electronic supplementary information (ESI) available. See DOI: 10.1039/d1sc04617a

‡ These authors have contributed equally to this work.

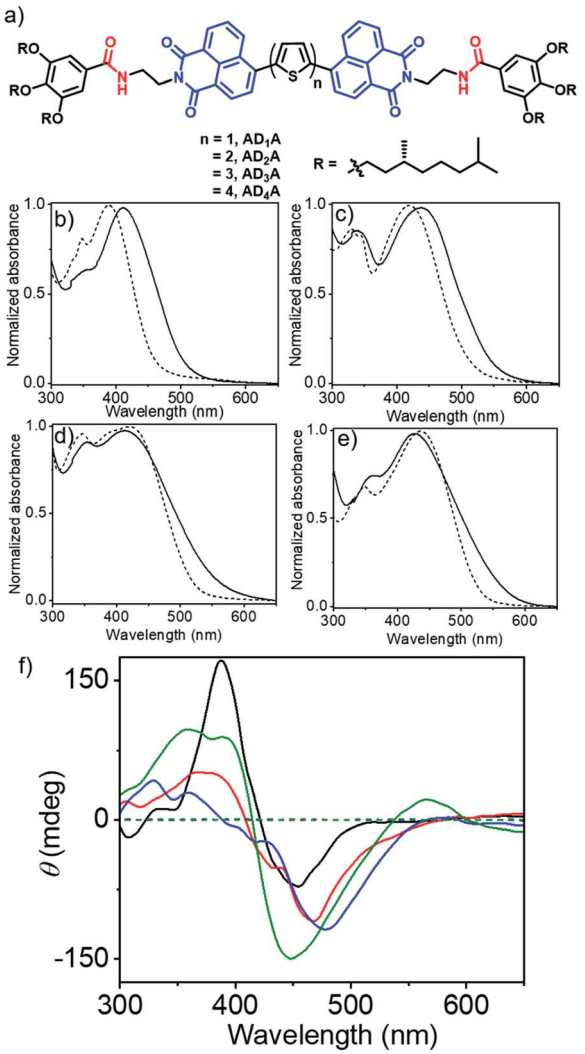

Fig. 1 (a) Structure of the bis-amide functionalized AD_nA molecules; UV/Vis spectra of (b) AD_1A, (c) AD_2A, (d) AD_3A and (e) AD_4A in 0.1 mM THF solution (broken lines) and in the film state (solid lines); (f) CD spectra of the AD_nA molecules in THF (broken lines) and MCH (solid lines). $c = 1.0$ mM, $l = 0.1$ cm. Black, red, blue and green lines represent AD_1A, AD_2A, AD_3A and AD_4A, respectively.

ambipolar systems (Fig. 1a)[18] in which naphthalimide and oligothiophene moieties serve as the A and D type chromophores, respectively. They are attached with two enantiopure trialkoxybenzamide wedges for the H-bonding driven chiral supramolecular polymerization,[14] as chirality too may influence the FE-polarization.[19] Herein we report H-bonding driven supramolecular polymerization of such AD_nA type ambipolar building blocks and its strong impact on stable ferroelectricity at ambient temperature with the highest saturation polarization (P_s) of ~2 μC cm^{-2} at a coercive field of about 2 kV cm^{-1}, which is the first observation of prominent ferroelectricity in any ambipolar chromophores. Further, we report the results of computational studies which provide the rationale for the origin of such prominent ferroelectricity in this unorthodox system (in the context of FEs).

Supramolecular assembly

Synthesis of an AD_4A (Fig. 1a) has been reported by us recently.[18] The other molecules shown in Fig. 1a were prepared following a similar procedure which is described in the ESI.† The cyclic voltammogram (CV) (Fig. S1†) of monomeric AD_nA molecules in THF (1.0 mM) showed peaks in the oxidation and reduction halves, suggesting their ambipolar nature. The quasi-reversible peaks in the reduction half and irreversible peaks in the oxidation half are assigned to the reduction of the naphthalimide and oxidation of the oligothiophene, respectively. The electrochemical bandgap (ΔE_{CV}), calculated from the onset of the first oxidation and reduction potentials, showed (Table 1) a gradual decrease from 2.49 eV to 2.31 eV with increasing oligothiophene length. Optical properties were investigated using the UV/Vis spectra (Fig. 1b) of the monomeric dye in THF and drop-cast thin films, obtained from the preformed aggregates in methyl-cyclohexane (MCH).[14] For the monomeric state, prominent absorption bands were noticed in the range of 300–500 nm with a gradual bathochromic shift going from AD_1A to AD_4A (Table 1), due to the increase in the conjugation length. For AD_1A and AD_2A, a significant bathochromic shift (23 nm and 20 nm, respectively) was noticed in the film-state compared to the corresponding spectrum in the THF solution, indicating an offset π-stacking, typically observed for naphthalimide derivatives.[14d]

In contrast, the hypsochromically shifted (~9 nm) absorption bands for the AD_3A and AD_4A systems with concomitant tailing at longer wavelengths indicate H-aggregation, generally observed for different oligothiophene-derivatives.[18,20] UV/Vis spectra in MCH (Fig. S2†) mostly resembled those in the film state, suggesting similar internal-order in the dried films. Photoluminescence spectra of the molecules were recorded in the monomeric (THF) and aggregated (MCH) states, which showed quenching of emission intensity in MCH (Fig. S3†), as typically reported for aggregation of different π-systems. The optical band gaps (ΔE_{UV}) of the AD_nA molecules were calculated from the onset of the absorption bands in the THF solution or in the solid film, respectively (Fig. 1b). In THF, the values match quite well with those estimated from the CV, while the reduced values in the aggregated state (Table 1) can be attributed to the π-stacking. The CD spectra (Fig. 1c) in MCH showed intense bands with a bi-signate Cotton effect, while no such band was noticed for the monomeric dye in THF, indicating chiral supramolecular assembly.[21]

The overlap of the zero cross-over point of the CD spectra (λ = 380–420 nm) with the absorption spectra of the corresponding dye in MCH (Fig. S2†) indicates exciton coupling. Temperature dependent CD experiments in MCH revealed (Fig. S5 and S6†) a gradual reduction of the CD band with increasing temperature. In case of all four molecules, an inflection point was noticed in the temperature range of 345–360 K, but in none of the samples did the CD band disappear completely even at the highest tested temperature suggesting only partial disassembly at elevated temperature.[22] Solvent-dependent FT-IR experiments revealed (Fig. S7†) a significant shift (200–

Table 1 Optical and electrochemical properties of the AD_nA molecules

	Optical properties					
	λ_{max} (nm, abs)			HOMO–LUMO energy gap [ΔE (eV)]		
Entry	THF	Solid	ε (mol^{-1} cm^{-1}, THF)	THF (UV)	THF (CV)	Solid (UV)
AD_1A	388	411	27 300	2.7	2.49	2.29
AD_2A	415	435	28 800	2.45	2.47	2.13
AD_3A	425	416	33 200	2.38	2.44	2.08
AD_4A	436	427	42 100	2.35	2.31	2.05

230 cm^{-1}) for the amide N–H stretching peaks toward lower wavenumber in MCH as compared to THF, suggesting a strong H-bonding in the aggregated state. FT-IR spectra of the samples in the solid state showed almost identical patterns compared to those observed in MCH, suggesting similar extent of H-bonding among the amide groups prevailing in MCH and in the solid state (Fig. S7†). Atomic force microscopy (AFM) images show (Fig. 2) a fibrillar morphology for the H-bonded supramolecular polymers of all four AD_nA molecules. Height and width of the small fibrils were estimated to be 3–4 nm and 100 nm, respectively, while the length extends over a few micrometres, revealing a long-range order. The presence of the thicker fibres can be attributed to the lateral clustering of the supramolecular polymer chains. An enlarged view of the selected region (insets, Fig. 2a and b) showed the existence of right-handed helical structures with helical pitch in the range of ~50–80 nm. The TEM image of a representative AD_2A sample showed a similar morphology (Fig. S8a†). SAED analysis was performed on the TEM image (inset, Fig. S8a†) and showed an amorphous nature as also indicated from the powder XRD (Fig. S8b†).

Ferroelectricity

To examine the presence and switchability of dipoles in the AD_nA supramolecular polymers, measurement of the dielectric constant (ε_r) was carried out between 300 K and 380 K with thick films (thickness ~ 0.1 mm) prepared on highly conductive ITO glass (Fig. S9†). Amongst the four molecules, AD_2A shows the highest ε_r value of ~44 at rt, and a clear ferroelectric–paraelectric phase transition at ~361 K can be noticed, where the ε_r value increases by about two-fold (Fig. 3a). The phase transition peak in this case can be typically correlated with the Curie temperature (T_c), which is typically observed in other organic and supramolecular ferroelectrics.[3,4,9,12] The permittivity of AD_2A near T_c could be linearly fitted to the Curie–Weiss law[23] (Fig. 3b), which confirms the true ferroelectric nature of the sample and the presence of switchable domains. The frequency independence of ε_r in the measured temperature range signifies that the orientations of the dipole moments follow the oscillating electric field.

That the prominent peak at T_c does not shift with varying frequency for AD_2A (Fig. 3c) is strong evidence of a transition

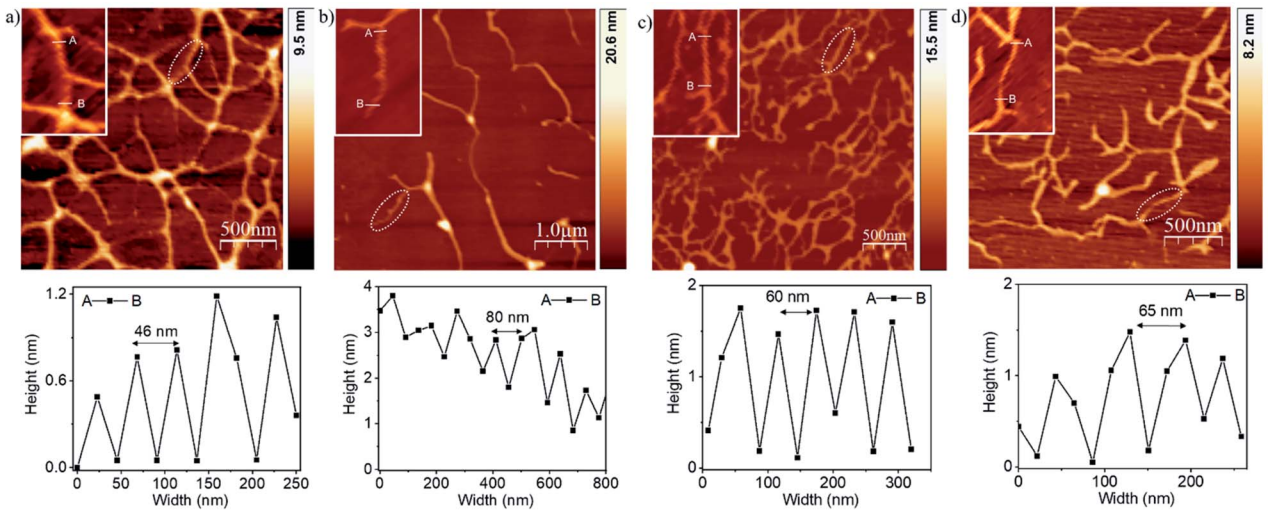

Fig. 2 AFM height images of supramolecular polymers of (a) AD_1A, (b) AD_2A, (c) AD_3A and (d) AD_4A. Samples were prepared by spin-coating an aggregated solution in MCH (0.1 mM) on freshly cut mica. The inset in each figure shows an enlarged view of a selected fibre (indicated by a white circle) with right-handed helicity. Height analysis along A–B in each zoomed-in image is shown in the bottom, confirming the helical nature of the fibres, and the helical pitch is estimated from the distance between two successive peaks.

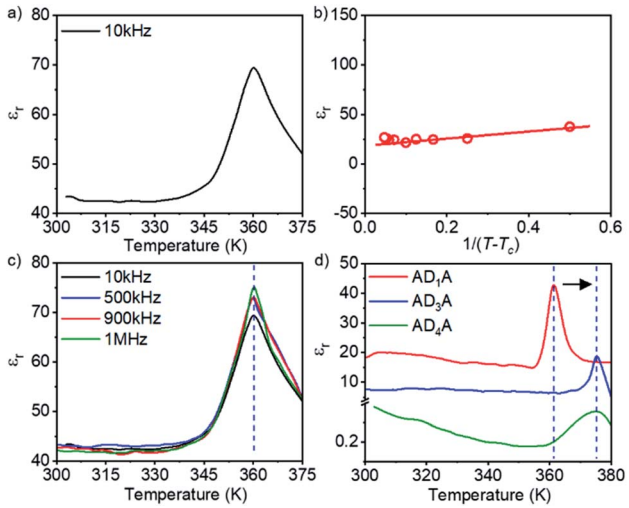

Fig. 3 (a) Anomalous dielectric permittivity (ε_r) at 10 kHz for the AD_2A film with increasing temperature showing the Curie temperature at 361 K; (b) Curie–Weiss fit near T_c for AD_2A; (c) dielectric permittivity peak (T_c) of AD_2A at different frequencies showing negligible deflection; (d) T_c shift to higher temperature in AD_3A and AD_4A films from AD_1A and AD_2A films.

from an order–disorder type ferroelectric to a paraelectric state in this system. This also rules out the presence of any relaxor behaviour in the molecule. Variants such as AD_1A show (Fig. 3d) a similar nature of dielectric behaviour as a function of increasing temperature with $T_c \sim 361$ K, but with a much lower ε_r value than that of AD_2A. Meanwhile, for AD_3A and AD_4A, the transition peaks shift to ~375 K (Fig. 3d), which may be attributed to the relatively higher temperature order–disorder change or partial disassembly in these molecules. Such a phase transition was further supported by micro-DSC experiments, which revealed a single endothermic peak at around 355–360 K for all four samples during the heating scan (Fig. S11†). For a representative sample (AD_2A), variable temperature UV/Vis studies in the film state revealed a partial disassembly at $T >$ 350 K (Fig. S12†), suggesting that the observed phase transition in DSC is related to this partial disassembly of the supramolecular polymers. It is noteworthy that even in MCH solution, a similar change was noticed in the UV/Vis spectra at a slightly lower temperature (Fig. S12 and S13†) compared to that in the solid state, suggesting not much difference in the self-assembly features in MCH or in the solid state which is also evident from their FT-IR spectra (Fig. S7†). As the change in ε_r was noticed at around the same temperature (Fig. 2), such partial disassembly of H-bonded supramolecular polymers near the T_c is proposed as a possible reason for the observed ferroelectric to paraelectric phase transition.

Direct and unambiguous evidence of the ferroelectricity was obtained through polarization *versus* electric field (*P–E*) hysteresis loops (Fig. 4), as polarization switching is the most common characteristic of ferroelectrics. *P–E* measurements at different temperatures were carried out from a capacitor configuration, with the AD_nA films sandwiched between top Ag electrode and bottom Ag/ITO electrodes (please see Fig. S10† for

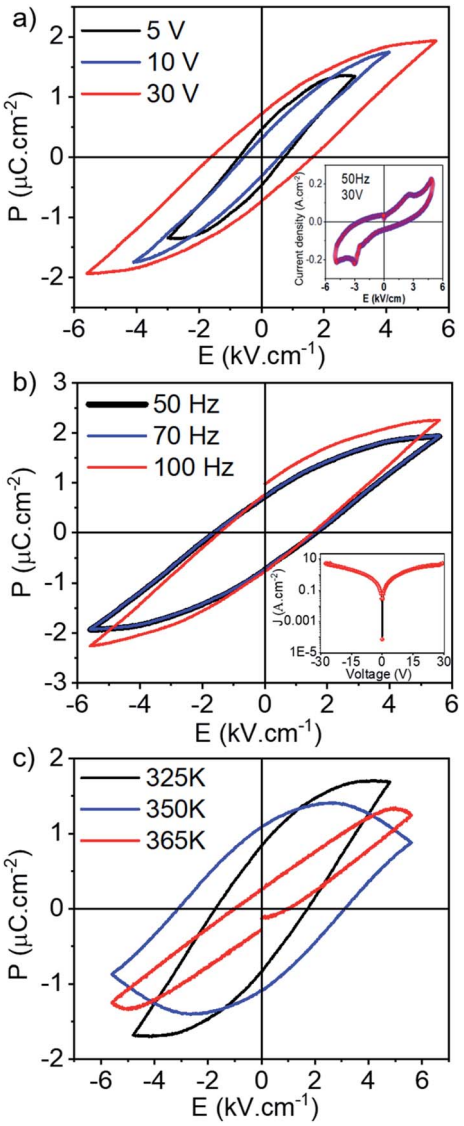

Fig. 4 (a) *P–E* hysteresis loops of the AD_2A film (50 Hz) at different applied voltages at 298 K. The inset shows the corresponding current–voltage loops (obtained during voltage sweeps where the voltage is cycled and the *P–E* hysteresis loops are recorded), showing clear switching peaks around the coercive voltage of the material. (b) Frequency dependence of polarization in the AD_2A film at 298 K and at an applied voltage of 30 V. The inset shows the leakage current density in the AD_2A film. (c) *P–E* hysteresis loops of the AD_2A film at different temperatures at 50 Hz.

SEM images). At 298 K, stable hysteresis loops with the highest saturation polarization (P_s) of ~1.9 μC cm^{-2}, $P_r \sim 0.5$ μC cm^{-2} and a maximum coercive field (E_c) of ≈1.6 kV cm^{-1} were obtained in the AD_2A film at 30 V applied voltage and at 50 Hz (Fig. 4a). The loops however show some contribution from dielectric loss and hence we also examined the switching current in the AD_2A systems (inset, Fig. 4a) to confirm the presence of ferroelectricity. The clear switching peaks visible in the *I–V* curve measured near the coercive field prove that the molecule is truly ferroelectric in nature.[3,24] We have also run PUND (Positive Up and Negative Down) sequences to measure

the switching charge density (Q_{SW}),[24] and a Q_{SW} value of ~0.5 μC cm^{-2} was measured from the AD_2A sample (Fig. S14†), further confirming a good ferroelectric response, matching with the remnant polarization value recorded from the sample (Fig. 4). The range of frequency dependence of polarization in the AD_2A film (Fig. 4b) reveals that P_s has almost no change up to 70 Hz as the slope remains unchanged. At 100 Hz, the value of P_s however increases to ~2.4 μC cm^{-2} even though the slope remains almost unchanged and the E_c increases within the measured frequency range from 70 Hz to 100 Hz. The inset of Fig. 4b shows the leakage current density *vs.* field of the AD_2A film, revealing a symmetric *I–V* behavior and a leakage current in the order of 0.8 A cm^{-2}. This implies that the ensuing polarization properties of the prepared capacitor film are not significantly affected by the leakage effects (Fig. S15†), again attributed to the similar intrinsic properties of the top and bottom electrodes, thereby proving the efficacy of the ferroelectric device structure. Comparing the *P–E* hysteresis loops measured at 350 K, a decrease in both the P_s and E_c can be found at the higher temperature and finally the ferroelectricity is lost beyond T_c at 365 K, showing thereafter a linear paraelectric behaviour (Fig. 4c and S16†). This phenomenon could be related to the disrupted long-range order of the polarization and the weakened coupling stabilizing effect between the charged defects and domains due to space-charge effects,[7,8] as well as the increased thermal fluctuations in the molecules at higher temperature.[25] To examine the effect of conjugation length, *P–E* measurements of the other AD_nA variants (AD_1A, AD_3A and AD_4A) were carried out (Fig. S17 and Table S1†). AD_1A was found to be the next best system with P_s ~ 1.1 μC cm^{-2} at 50 Hz. In contrast, AD_3A and AD_4A exhibited signatures of unstable ferroelectricity and ill-developed hysteresis loops with lower values of polarization (~0.7 μC cm^{-2} in AD_3A and ~0.07 μC cm^{-2} in AD_4A at 50 Hz) as compared to AD_2A at an extremely low electric field (≪1 kV cm^{-1}) (Fig. S17†). On further increasing the electric field, polarization was destroyed in these samples except in AD_1A (but it became lossy at higher field). While the difference between AD_1A and AD_2A may be attributed to their intrinsic difference in molecular structure, the sharp decline in the FE-properties of AD_3A and AD_4A may be related to the difference in the internal order as in these two cases the spectral shift suggested H-type aggregation, in contrast to the other two molecules which showed bathochromically shifted absorption bands in the film state compared to those of the monomeric dye in THF solution (Fig. 1b and Table 1).

While the comparison between different AD_nA molecules highlights the importance of the intrinsic molecular structure, to examine the importance of the supramolecular organization and the presence of the ambipolar π-system itself to the ferroelectricity, two control molecules (C1 and C2, Fig. 5a) were studied. C1 contains the same conjugated chromophore as in the best performing AD_2A system (Fig. 1a), but not the amide groups for H-bonding driven supramolecular assembly. On the other hand, C2 with the same amide-functionalized chiral wedge lacks any AD_nA-chromophore. Solvent dependent UV/Vis and CD spectra (Fig. S18†) of C1 confirmed no specific supramolecular assembly in MCH, in sharp contrast to AD_2A, as

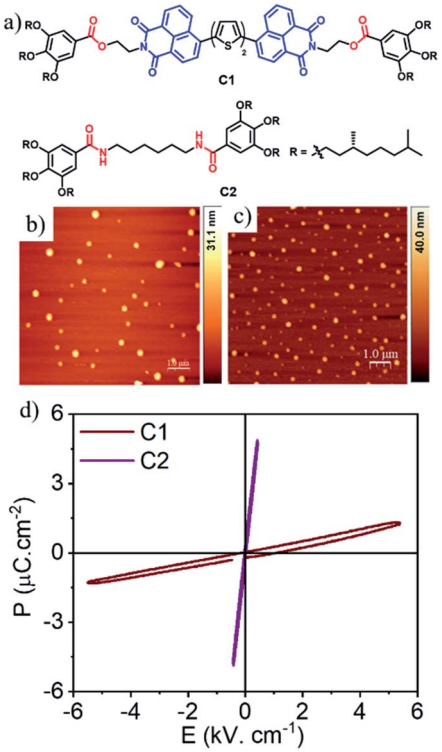

Fig. 5 (a) Structure and (b and c) AFM images of C1 and C2. (c and d) Absence of ferroelectricity in C1 and C2 at 50 Hz.

expected in the absence of H-bonding. On the other hand, H-bonding between the amide groups in C2 was evident from the FT-IR spectra (Fig. S19†), but it has no ambipolar chromophore. AFM images (Fig. 5b and c) showed a spherical morphology (Fig. 2) for both samples in contrast to the fibrillar structures of the amide containing AD_nA molecules. Fig. 5d reveals C1 to be a non-ferroelectric compound, in which a rather tight dielectric signal is measured at rt.[25] Likewise, C2 also does not exhibit any FE-polarization; rather, it shows a typical dielectric *P–E* response, which underscores the essential role of the molecular structure as well as the H-bonded supramolecular assembly in the observed outstanding FE-polarization of the present AD_2A system.

Discussion and computational studies

Overall, the present example of the supramolecular polymer of AD_2A shows a significant improvement in terms of ferroelectric parameters (P_s, coercive field) in comparison to some of the best examples of organic FE systems reported to date.[3–6,11,12] The low E_c value in the AD_2A system as compared to those of other reported FE organic perovskites (~10 kV cm^{-1})[26] or polymers such as PVDF (500 kV cm^{-1})[5] makes this newly introduced ambipolar π-system attractive for future low power applications. It is proposed that the polarizability of the AD_nA-chromophores creates a partial charge-separation while the extended H-bonding enables the long-range order, which together contribute to the observed exceptional FE-polarization at rt. The

ferroelectricity might stem from the displacive motion of the central donor moiety (δ^+) between the two terminal acceptors (δ^-) accompanied by an order–disorder structural change. To better understand the origin of the ferroelectricity, computational studies were performed with the representative AD_2A system. Fig. 6a shows the optimized geometry of the representative tetrameric stack of the best performing AD_2A system (without the peripheral chains) which reveals an average stacking distance of ~4 Å. The N–H···O=C H-bonds formed between two adjacent layers play a major role in stabilizing the stacked structures. It is seen that the C=O of the amide group of one molecule interacts with the N–H of the amide group of the adjacent molecule *via* H-bonds with bond distances of 1.95 Å, 1.83 Å and 1.93 Å along one edge while the corresponding distances are 2.22 Å, 2.63 Å and 2.62 Å towards another edge. Similar optimized structures were obtained for the dimer and the octamer as well (Fig. S20†), through semi-empirical PM6 calculations. Electron density mapping for the tetramer is shown in Fig. 6b from ESP calculations. The isosurface colour coded with the electrostatic potential shows a red region which indicates an electron dense domain while the electron deficient domain is indicated in blue. With increasing stacking, electron transfer occurs towards the edges from the electron-rich region containing corner-sharing thiophene units, making it relatively positive. Such charge separation should result in a significant dipole moment and polarization for the aggregates. The dipole moment (in Debye) has been computed for each of the AD_2A oligomers (see the ESI† for details).[27] Fig. S21† shows the change in the average dipole moment (μ) with an increase in the number of stacked molecules (n). Going from the dimer to the tetramer, a significant increase in the μ can be noticed (from about 4 to 11 Debye) which is further increased in the octameric stack, which provides an important clue to the origin of the ferroelectricity specifically in the supramolecular assembly of AD_2A but not for the monomeric dye (C1, Fig. 5) in the absence of H-bonding. Additionally, the structural changes in AD_2A on heating were studied using ReaxFF simulations (see the Computational section, ESI†). The interlayer sulphur···sulphur distances in bithiophene and stacking side-chain distances are plotted with increasing temperature (Fig. S22†).

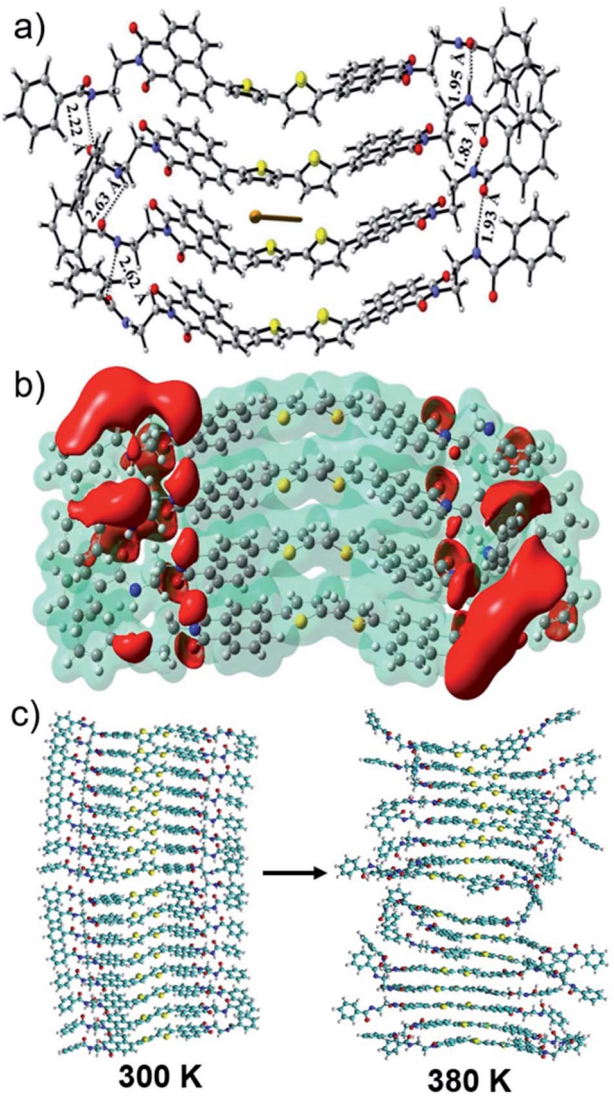

Fig. 6 (a) Optimized structure of the tetramer of AD_2A. Peripheral alkyl chains have been removed during optimization. The arrow shows the direction of the dipole moment for each case; (b) 3D plot of the ESP of the tetramer of AD_2A; (c) snapshots of structural reorganization of the AD_2A aggregate as the temperature is increased from 300 K to 380 K from ReaxFF simulations.

As the temperature is progressively increased, the average S···S distance increases from ~4.4 Å to ~5.2 Å at 350 K. Similarly, the interlayer stacking distance between the side-chains also increases from ~4.3 Å (at 300 K) to ~5.5 Å at 350 K. Clearly, the AD_2A aggregate becomes more disordered as the temperature increases (Fig. 6c). These results are consistent with the experimental results from DSC and variable temperature UV/Vis experiments and therefore further support the hypothesis regarding partial disassembly of the supramolecular polymers at elevated temperature which has been proposed as a possible reason for the ferroelectric to paraelectric phase transition in these systems.

Conclusions

We have demonstrated highly promising and stable ferroelectricity up to 350 K ($T_c \sim 361$ K) in the H-bonded supramolecular polymers of ambipolar π-systems with a saturation polarization of ~2.0 μC cm^{-2} at a low coercive field of ~2 kV cm^{-1}. This is a significant value reported for any supramolecular system and is comparable to those of existing low-cost organic ferroelectrics. Although two-component CT-complexes have been known for moderate FE-polarization at rt, the scope for further improving their utility by exploring wider structural variants[28] may be limited due to the difficulty in achieving precise spatial control in complex multi-component supramolecular assemblies. In this context the outstanding FE-polarization, reported herein for a single-component ambipolar π-system, is a significant step forward and may inspire the exploration of already familiar wide-ranging ambipolar scaffolds for soft-ferroelectrics.

Author contributions

Suhrit Ghosh and Anuja Datta jointly conceptualized and supervised the work and raised external funding support. Ayan Datta supervised the computational studies. AM and SC carried out the synthesis, characterization and supramolecular assembly studies of the molecules. SB performed the dielectric, ferroelectric and leakage current measurements. AG performed the computational analysis. All co-authors contributed to the manuscript preparation.

Conflicts of interest

There are no conflicts to declare.

Acknowledgements

AM, SB, AG and SC thank CSIR-India for a research fellowship. AD acknowledges the SERB Ramanujan Fellowship (SB/S2/RJN-0057/2017) for financial support. SG and AD thank SERB for funding (Grant No.: CRG/2020/002395). Authors thank Dr Devajyoti Mukherjee, SPS, IACS for providing access to the dielectric measurement facilities and Professor Priyadarsi De, IISER Kolkata, for assistance with the DSC measurements.

Notes and references

1 L. W. Martin and A. M. Rappe, *Nat. Rev. Mater.*, 2016, **2**, 16087.
2 J. Valasek, *Phys. Rev.*, 1921, **17**, 475.
3 (*a*) C. Park, K. Lee, M. Koo and C. Park, *Adv. Mater.*, 2020, e2004999; (*b*) A. S. Tayi, A. Kaeser, M. Matsumoto, T. Aida and S. I. Stupp, *Nat. Chem.*, 2015, **7**, 281; (*c*) S. Horiuchi and Y. Tokura, *Nat. Mater.*, 2008, **7**, 357; (*d*) S. Horiuchi, R. Kumai and Y. Tokura, *Chem. Commun.*, 2007, 2321.
4 (*a*) J. Harada, Y. Kawamura, Y. Takahashi, Y. Uemura, T. Hasegawa, H. Taniguchi and K. Maruyama, *J. Am. Chem. Soc.*, 2019, **141**, 9349; (*b*) Y. Ai, D.-J. Wu, M.-J. Yang, P. Wang, W.-H. He and W.-Q. Liao, *Chem. Commun.*, 2020, **56**, 7033.
5 B. Stadlober, M. Zirkl and M. Irimia-Vladu, *Chem. Soc. Rev.*, 2019, **48**, 1787.
6 (*a*) K. Kishikawa, S. Nakahara, Y. Nishikawa, S. Kohmoto and M. Yamamoto, *J. Am. Chem. Soc.*, 2005, **127**, 17962; (*b*) C. F. C. Fitié, W. S. C. Roelofs, M. Kemerink and R. P. Sijbesma, *J. Am. Chem. Soc.*, 2010, **132**, 6892; (*c*) D. Miyajima, F. Araoka, H. Takezoe, J. Kim, K. Kato, M. Takata and T. Aida, *Science*, 2012, **336**, 209; (*d*) I. Urbanaviciute, X. Meng, T. D. Cornelissen, A. V Gorbunov, S. Bhattacharjee, R. P. Sijbesma and M. Kemerink, *Adv. Electron. Mater.*, 2017, **3**, 1600530; (*e*) H. Anetai, T. Takeda, N. Hoshino, H. Kobayashi, N. Saito, M. Shigeno, M. Yamaguchi and T. Akutagawa, *J. Am. Chem. Soc.*, 2019, **141**, 2391.
7 (*a*) M. Dawber, K. M. Rabe and J. F. Scott, *Rev. Mod. Phys.*, 2005, **77**, 1083; (*b*) J. F. Scott, *Science*, 2007, **315**, 954; (*c*) A. Datta, D. Mukherjee and S. Kar-Narayan, in *Metal Oxide-Based Thin Film Structures: Formation, Characterization and Application of Interface-Based Phenomena*, ed. N. Pryds and V. Esposito, Elsevier, 2018, pp. 465–488; (*d*) Z. Fan, K. Sun and J. Wang, *J. Mater. Chem. A*, 2015, **3**, 18809.
8 (*a*) A. Datta, P. E. Sanchez-Jimenez, R. A. R. Al Orabi, Y. Calahorra, C. Ou, S.-L. Sahonta, M. Fornari and S. Kar-Narayan, *Adv. Funct. Mater.*, 2017, **27**, 1701169; (*b*) A. Datta, D. Mukherjee, C. Kons, S. Witanachchi and P. Mukherjee, *Small*, 2014, **10**, 4093; (*c*) A. Datta, D. Mukherjee, S. Witanachchi and P. Mukherjee, *Adv. Funct. Mater.*, 2014, **24**, 2638; (*d*) D. J. Singh, M. Ghita, M. Fornari and S. V Halilov, *Ferroelectrics*, 2006, **338**, 73.
9 (*a*) Y.-Y. Tang, P.-F. Li, W.-Y. Zhang, H.-Y. Ye, Y.-M. You and R.-G. Xiong, *J. Am. Chem. Soc.*, 2017, **139**, 13903; (*b*) W.-J. Xu, K. Romanyuk, J. M. G. Martinho, Y. Zeng, X.-W. Zhang, A. Ushakov, V. Shur, W.-X. Zhang, X.-M. Chen, A. Kholkin and J. Rocha, *J. Am. Chem. Soc.*, 2020, **142**, 16990.
10 (*a*) A. Das and S. Ghosh, *Angew. Chem., Int. Ed.*, 2014, **53**, 2038; (*b*) M. Kumar, K. Venkata Rao and S. J. George, *Phys. Chem. Chem. Phys.*, 2014, **16**, 1300.
11 (*a*) S. Horiuchi, R. Kumai and Y. Tokura, *J. Am. Chem. Soc.*, 1998, **120**, 7379; (*b*) F. Kagawa, S. Horiuchi, M. Tokunaga, J. Fujioka and Y. Tokura, *Nat. Phys.*, 2010, **6**, 169; (*c*) K. Kobayashi, S. Horiuchi, R. Kumai, F. Kagawa, Y. Murakami and Y. Tokura, *Phys. Rev. Lett.*, 2012, **108**, 237601.
12 (*a*) A. S. Tayi, A. K. Shveyd, A. C.-H. Sue, J. M. Szarko, B. S. Rolczynski, D. Cao, T. J. Kennedy, A. A. Sarjeant, C. L. Stern, W. F. Paxton, W. Wu, S. K. Dey, A. C. Fahrenbach, J. R. Guest, H. Mohseni, L. X. Chen, K. L. Wang, J. F. Stoddart and S. I. Stupp, *Nature*, 2012, **488**, 485; (*b*) A. Narayanan, D. Cao, L. Frazer, A. S. Tayi, A. K. Blackburn, A. C.-H. Sue, J. B. Ketterson, J. F. Stoddart and S. I. Stupp, *J. Am. Chem. Soc.*, 2017, **139**, 9186; (*c*) M. Pandeeswar, S. P. Senanayak, K. S. Narayan and T. Govindaraju, *J. Am. Chem. Soc.*, 2016, **138**, 8259.
13 H. Kar and S. Ghosh, *Isr. J. Chem.*, 2019, **59**, 881.
14 (*a*) T. F. A. De Greef, M. M. J. Smulders, M. Wolffs, A. P. H. J. Schenning, R. P. Sijbesma and E. W. Meijer, *Chem. Rev.*, 2009, **109**, 5687; (*b*) F. Würthner, C. R. Saha-Möller, B. Fimmel, S. Ogi, P. Leowanawat and D. Schmidt, *Chem. Rev.*, 2016, **116**, 962; (*c*) S. S. Babu, V. K. Praveen and A. Ajayaghosh, *Chem. Rev.*, 2014, **114**, 1973; (*d*) C. Rest, R. Kandanelli and G. Fernández, *Chem. Soc. Rev.*, 2015, **44**, 2543–2572; (*e*) A. Das and S. Ghosh, *Chem. Commun.*, 2016, **52**, 6860.
15 F. Würthner, *Acc. Chem. Res.*, 2016, **49**, 868.
16 H. Jiang, *Macromol. Rapid Commun.*, 2010, **31**, 2007.
17 (*a*) A. Saeki, Y. Koizumi, T. Aida and S. Seki, *Acc. Chem. Res.*, 2012, **45**, 1193; (*b*) J. Zhao, C. Yao, M. U. Ali, J. Miao and H. Meng, *Mater. Chem. Front.*, 2020, **4**, 3487; (*c*) R. Stalder, S. R. Puniredd, M. R. Hansen, U. Koldemir, C. Grand, W. Zajaczkowski, K. Müllen, W. Pisula and J. R. Reynolds, *Chem. Mater.*, 2016, **28**, 1286; (*d*) T. Duan, H. Tang, R.-Z. Liang, J. Lv, Z. Kan, R. Singh, M. Kumar, Z. Xiao, S. Lu and F. Laquai, *J. Mater. Chem. A*, 2019, **7**, 2541; (*e*) X. Liu, Y. Sun, L. A. Perez, W. Wen, M. F. Toney, A. J. Heeger and G. C. Bazan, *J. Am. Chem. Soc.*, 2012, **134**,

20609; (*f*) S. Prasanthkumar, A. Gopal and A. Ajayaghosh, *J. Am. Chem. Soc.*, 2010, **132**, 13206.

18 S. Chakraborty, S. Varghese and S. Ghosh, *Chem.–Eur. J.*, 2019, **25**, 16725.

19 (*a*) A. Seki, M. Yoshio, Y. Mori and M. Funahashi, *ACS Appl. Mater. Interfaces*, 2020, **12**, 53029; (*b*) P.-F. Li, W.-Q. Liao, Y.-Y. Tang, W. Qiao, D. Zhao, Y. Ai, Y.-F. Yao and R.-G. Xiong, *Proc. Natl. Acad. Sci.*, 2019, **116**, 5878.

20 A. Mishra, C.-Q. Ma and P. Bäuerle, *Chem. Rev.*, 2009, **109**, 1141.

21 (*a*) A. R. A. Palmans and E. W. Meijer, *Angew. Chem., Int. Ed.*, 2007, **46**, 8948; (*b*) P. Duan, H. Cao, L. Zhang and M. Liu, *Soft Matter*, 2014, **10**, 5428.

22 G. Pescitelli, D. Padula and F. Santoro, *Phys. Chem. Chem. Phys.*, 2013, **15**, 795.

23 B. Jaffe, W. Cook and H. Jaffe, in *Non-Metallic Solids, Piezoelectric Ceramics*, ed. J. P. Roberts and P. Popper, Academic Press, London, 1971.

24 (*a*) K. M. Rabe, C. H. Ahn and J.-M. Triscone, *Physics of Ferroelectrics: a Modern Perspective*, Springer Berlin Heidelberg, Berlin, Heidelberg, 2007; (*b*) M. Dawber, K. M. Rabe and J. F. Scott, *Rev. Mod. Phys.*, 2005, **77**, 1083–1130.

25 (*a*) D. Damjanovic, Hysteresis in Piezoelectric and Ferroelectric Materials, in *The Science of Hysteresis*, ed. G. Bertotti and I. Mayergoyz, Academic Press, Oxford, 2006, pp. 337–465; (*b*) L. Jin, F. Li and S. Zhang, *J. Am. Ceram. Soc.*, 2014, **97**, 1.

26 H.-Y. Ye, Y.-Y. Tang, P.-F. Li, W.-Q. Liao, J.-X. Gao, X.-N. Hua, H. Cai, P.-P. Shi, Y.-M. You and R.-G. Xiong, *Science*, 2018, **361**, 151.

27 Y. Wang, P. Verma, X. Jin, D. G. Truhlar and X. He, *Proc. Natl. Acad. Sci.*, 2018, **115**, 10257.

28 S. Chen and X. C. Zeng, *J. Am. Chem. Soc.*, 2014, **136**, 6428.